Blowdown Pulser Design Criteria for Solid-Propellant Rockets

R. S. Brown*
United Technologies Chemical Systems Division, San Jose, California

Pulsing solid-propellant rocket motors is often employed to evaluate the stability of the combustion pressure. The time constant of the exponentially decaying oscillations generated by the pulser provides a quantitative measure of the linear stability of the combustion pressure. Experience has shown that current design methods are inadequate for estimating the pulser charge and action time required to generate a specified pulse amplitude. This paper describes analytical and experimental studies to develop improved design methods. The linearized equations for the transient ballistics of the combustion chamber and the blowdown pulser have been solved using a Fourier transform approach. The analysis shows the exponential decay time for a blowdown pulser should be approximately twice the frequency of interest. The analysis also shows the initial pulse amplitude scales linearly with the ratio of initial pulser mass flow to motor mass flow. To generate an 8% peak-to-peak pulse amplitude requires that this ratio be approximately unity. Cold-flow experiments show the observed trends of pulse amplitude with pulser mass flow and blowdown time agree reasonably well with the predicted trends. However, the observed pulse amplitudes are slightly higher than the predicted amplitudes.

Nomenclature

a = sonic velocity
A = acoustic admittance
B = integration constant
c^* = characteristic velocity
C = $0.5(\mathrm{d}\bar{M}/\mathrm{d}Z)(Q+i\lambda-A_bqL/S+2\mathrm{d}\bar{M}/\mathrm{d}Z)$
d = diameter
D = thermal diffusivity
E = parameter in combustion response function
f = frequency
F' = particle damping term
G = parameter in combustion response function
H = Fourier transform
I = integration constant
i = square root of -1
k = $(i\lambda-A_bqL/S)(Q+\mathrm{d}\bar{M}/\mathrm{d}Z)/4C$
K = Kummer function, $K(a,b,c)$
L = chamber length
m = mass flow rate
M = Mach number
n = burning rate pressure exponent
N = $Da/(L\dot{r}_0^2)$
P = pressure
q = chamber perimeter
Q = $i(1+C_m+i\lambda\tau_d)/(1+i\lambda\tau_d)+(1-R_{ft})(\mathrm{d}\bar{M}/\mathrm{d}Z)$
Q = $f/\Delta f$
r = CZ^2
$\dot{r}$ = propellant burning rate
R = response function
S = area
T = see Eq. (8)
V = volume
W = $K(k+1,3/2,r)/K(k,\frac{1}{2},r)$
Z = dimensionless chamber length
α = exponential time constant
γ = specific heat ratio
ϵ = acoustic pressure, $P'/\gamma\bar{P}$
λ = dimensionless frequency, $2\pi fL/a$
ω_f = dimensionless flame temperature
ρ = density
σ' = flow turning parameter, $M'\,\mathrm{d}\bar{M}/\mathrm{d}Z$
τ = dimensionless time, ta/L
τ_d = particle damping parameter, $ad_p^2\rho_p/(18\mu L)$
ψ = $\psi(\psi-1)=iN$

Subscripts

0 = at $Z=0$
1 = at $Z=1$
b = burning
c = chamber
d = damping
ft = flow turning
p = pulser

Superscripts

([ ) = time average
( )' = oscillating
$\circ$ = initial
($\tilde{}$) = Fourier transform

Introduction

PULSING of solid-propellant rocket motors has been used for many years as a method for measuring the stability of the combustion pressure. For example, the Booster Separation Motor[1] and the simulator for the small Inertial Upper Stage[2] were pulsed to measure their stability properties. Other organizations have also pulsed many of their motors during development for the same reasons. Experience from these programs has shown the need for improved pulser design methods.

Several years ago, Murray[3] conducted the first in a series of programs to improve pulser design methods. However, the results from this initial program did not provide the necessary improvements. This led to later studies by Baum et al.[4-6] that investigated a nonlinear time domain model for analyzing pulser performance. Both ejecta and blowdown pulsers were analyzed and reasonable agreement between the predicted and observed behavior was demonstrated. While extremely useful, this model does not provide the simplified equations needed to develop the scaling criteria and design guidelines relating pulser behavior and the chamber ballistics. Therefore, the present study was undertaken to evaluate a simplified model of pulser behavior that could provide simplified design guidelines and scaling criteria.

Received April 14, 1985.

*Senior Staff Scientist. Associate Fellow AIAA.

Analytical Model Development

There are two basic elements to be considered in predicting the response of a combustion chamber to a disturbance produced by a pulser: 1) the nature of the disturbance produced by the pulser and 2) the response of the chamber to that disturbance. The approach taken in this study is to derive a separate simplified analysis for each of these elements. Specifically, the Fourier transforms for both the linearized pulser ballistics and the chamber response are developed. The product of these two transforms is the transform of the chamber pressure response. By inverting the product, the time domain behavior of the acoustic pressure can be predicted.

The equations for the dynamics of the combustion chamber can be approximated by starting with the one-dimensional equations of motion. After linearization and rearrangement, one obtains, after Culick,[7,8]

$$\frac{\partial \epsilon'}{\partial Z}+\frac{\partial M'}{\partial \tau}+\frac{\partial(\bar{M}M')}{\partial Z}+\sigma'-F'=0 \tag{1}$$

for the momentum equation and

$$\frac{\partial \epsilon'}{\partial \tau}+\frac{\bar{M}\partial \epsilon'}{\partial Z}+\frac{\partial M'}{\partial Z}=\left(\frac{A_b qL}{S}\right)\epsilon' \tag{2}$$

for the energy equation. These equations include flow turning losses σ', particle damping losses F', and the pressure coupled acoustic admittance of the propellant A_b. The velocity coupling terms have been omitted to simplify the equations. However, methods for including velocity coupling effects have been developed,[9] so this simplification is not a basic limitation of the analysis.

Assuming oscillatory behavior, the time derivatives can be replaced by $i\lambda$. Equations (1) and (2) are thereby transformed to the frequency domain and can then be rearranged to form the classical wave equation, which can then be transformed into a Kummer equation,[9-11]

$$r^2 \mathrm{d}^2\tilde{\epsilon}/\mathrm{d}r^2+(0.5-r)\mathrm{d}\tilde{\epsilon}/\mathrm{d}r-k\tilde{\epsilon}=0 \tag{3}$$

The solution to Eq. (3) can then be written in terms of Kummer functions

$$\tilde{\epsilon}=B^*K(k,\tfrac{1}{2},r)+I^*K(k+1,3/2,r) \tag{4}$$

The transform of the acoustic Mach number can then be determined from

$$\tilde{M}=\left[\bar{M}\left(i\lambda-\frac{A_b qL}{S}\right)-\frac{\mathrm{d}\tilde{\epsilon}}{\mathrm{d}Z}\right]/Q \tag{5}$$

The integration constants B and I are determined from the boundary conditions at each end of the motor. In this particular model, the pulser has been located at the aft end of the motor to avoid a gross violation of a basic assumption in the linearized equations. Specifically, in linearizing Eq. (1), $M' \ll \bar{M}$ has been assumed to apply throughout the chamber. When the chamber is pulsed, however, M' is likely to be large compared to $\bar{M}$, particularly if the pulser is located at the head end. Locating the pulser at the aft end where $\bar{M}$ is much larger minimizes inaccuracies in the model resulting from this assumption. Thus, in this model at $Z=0$, $\tilde{M}=0$ and, therefore, $I=0$.

Since $K(k,\tfrac{1}{2},0)=1$, Eq. (4) becomes

$$\tilde{\epsilon}=\tilde{\epsilon}_0 K(k,\tfrac{1}{2},r) \tag{6}$$

Furthermore, Eq. (5) can be simplified to

$$\tilde{M}/\bar{M}=T(\lambda,r) \tag{7}$$

where

$$T(\lambda,r)=\left(\frac{A_b qL}{S}-i\lambda\right)\frac{[Q^*W-(\mathrm{d}\bar{M}/\mathrm{d}Z)(1-W)]}{Q^*(\mathrm{d}\bar{M}/\mathrm{d}Z)} \tag{8}$$

At the aft end ($Z=1$), a simple mass balance for the time dependent flow becomes

$$\frac{\tilde{M}}{\bar{M}}-0.5(\gamma-1)=\left(\frac{\tilde{m}_p}{\dot{m}_p^\circ}\right)\left(\frac{\dot{m}_p^\circ}{\dot{m}_c}\right) \tag{9}$$

Note that a positive pulser mass flow has been defined as flowing from the motor chamber into the pulser. This definition is arbitrary since pulses can be generated by flow in either direction. In Eq. (9), the motor exhaust nozzle is assumed to follow isentropic quasisteady-state behavior.†

After substituting Eq. (7) into Eq. (9), the equation for the Fourier transform of the aft-end acoustic pressure normalized to the pulser flow becomes

$$\tilde{\epsilon}_1=\frac{(\dot{m}_p/\dot{m}_{pc}^\circ)(\dot{m}_p/\dot{m}_{pp}^\circ)}{T(\lambda,r)-0.5(\gamma-1)} \tag{10}$$

If the Fourier transform of the pulser mass flow is known, the time domain behavior of the aft-end acoustic pressure can be obtained by inverting Eq. (10).

In this study, a novel approach was taken to solving this model. The frequency domain equations (6-10) were programmed on a Hewlett-Packard model 9825T laboratory computer. The frequency bandwidth of interest was then selected and numerical values of the Fourier transform calculated to form the discrete transform. The discrete transform was transferred through the computer interface to a Hewlett-Packard model 5420A spectrum analyzer. The time domain pressure was then obtained using the inversion routine in the analyzer. The results were displayed using the plotting routine in the analyzer.

Verification of Solution

A series of calculations were made to verify the programming and to validate the calculational procedure. In the simplest case, the propellant burning rate and flame temperature from a side burning grain were assumed to be independent of the acoustic pressure, i.e., $A_b=-\gamma\bar{M}_b$. As the frequency approaches zero, the Kummer functions approach unity and hence

$$T(\lambda,r)\to\gamma \tag{11}$$

Furthermore, one would expect $T(\lambda,r)$ to show peak values at the resonant frequencies of $0.5n$, where $n=1,2,3\ldots$. If no particle damping effects are present, one would also expect the values at these peaks to be independent of frequency. Figure 1 shows the magnitude of the predicted Fourier transform of the head end acoustic pressure for the conditions described above (assuming a unit impulse-type pulser) yields the expected characteristics. As an additional check, the half-power bandwidth of these peaks, Q, was calculated to be 28.9 with $\gamma=1.4$ and $\mathrm{d}\bar{M}/\mathrm{d}Z=0.0285$. This compares to a value of 29 predicted by one-dimensional stability theory.[7,8]

Another check was obtained by examining the predicted behavior of the equations at frequencies below 0.2. Here one would expect the oscillatory pressures to be in phase and to have the same amplitude throughout the motor, i.e., bulk mode behavior. Thus, these equations should become identical to the bulk mode equations developed for the rotating valve experiment.[9,11] At low frequencies, the Kummer func-

†This assumption relates the temperature oscillation at the nozzle entrance to the pressure oscillation at the nozzle. It is really used for convenience in most stability analyses because it avoids the need to analyze for convected temperature (i.e., entropy) waves.

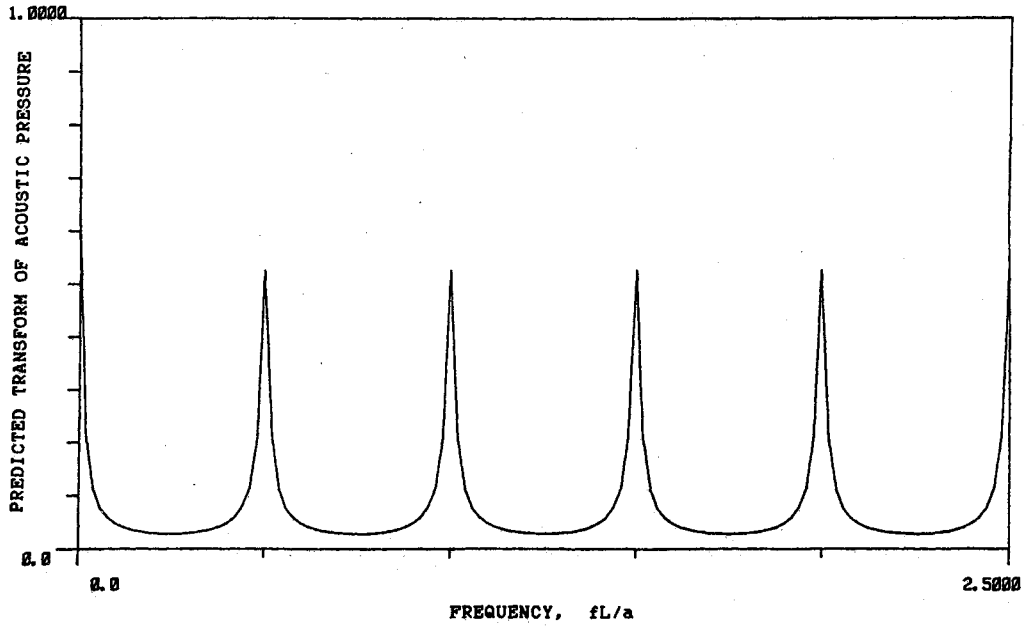

Fig. 1 Predicted magnitude of transform cold flow.

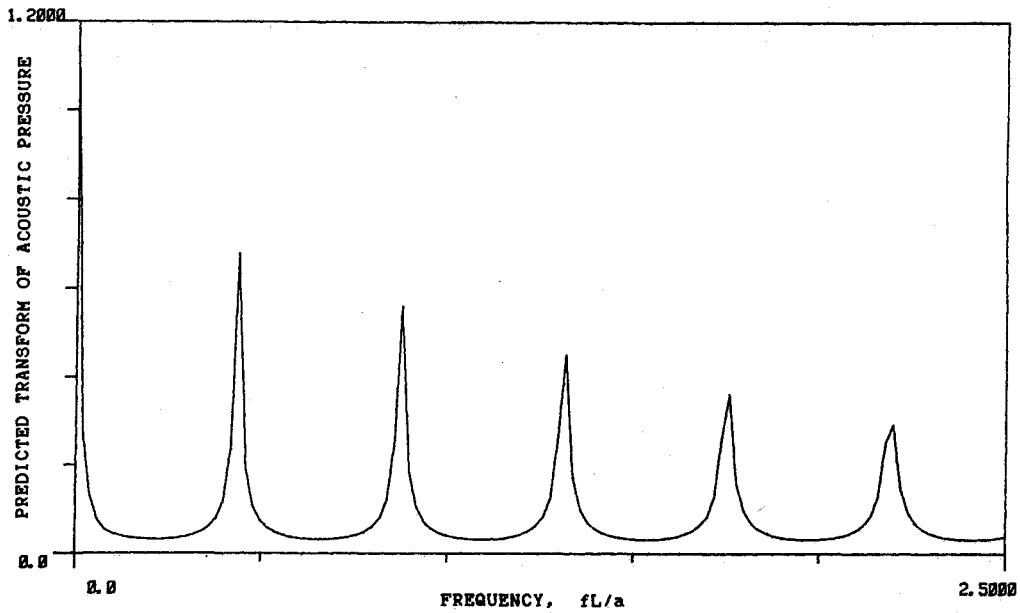

Fig. 2 Predicted magnitude of transform, combustion.

tions are unity. Equations (7-9) can then be easily simplified and shown to be identical to the equations describing bulk mode behavior.

Numerical experiments were then conduced to examine the predicted behavior under combustion conditions. To make these calculations, the dynamic response of the propellant was simulated by the classical one-dimensional equation for the acoustic response function[12]

$$A_b = \gamma \bar{M}_b \left[\frac{n(1+E-G)}{(\psi + E/\psi - G)} - 1 \right] \tag{12}$$

Table 1 shows values for the coefficients derived by curve fitting Eq. (12) to rotating valve and T-burner data.[13] Particle damping parameters were derived from the propellant composition and T-burner data. Figure 2 shows the spectra of the normalized transform of the head end acoustic pressure, again assuming a unit impulse-type pulser. Note that the peak values decrease and the half-power bandwidths increase with increasing frequency. Note also that the resonant frequencies have shifted from multiples of 0.5, the classical organ pipe frequencies. All of these characteristics are expected from the increased damping with increasing frequency and the phase shifts from the dynamic response and particle damping.

Table 1 Combustion coefficients for a typical propellant

$n=0.27$	$d\bar{M}/dZ=0.0285$
$E=15.0$	$\gamma=1.1$
$G=4.97$	$\gamma_d=0.002$
$N=31.7$	$C_m=0.30$

Analysis of Powder Pulsers

Powder pulsers are one of the most commonly used methods for generating mass flow disturbances in rocket motors. In this type of pulser, a charge of gun powder is ignited by a squib and the combustion products pressurize a breech chamber. Eventually, the breech pressure overstresses a burst disk, which then ruptures. The breech gases vent into the motor chamber, creating a momentary increase of gas flow into the motor. Assuming the breech pressure to be substantially higher than the motor pressure, one would expect the breech exhaust to be sonically choked and thereby the breech

pressure to decay exponentially. An approximate mass balance for the pulser breech can be written

$$\left(\frac{\alpha V_p}{L}\right)\frac{d\rho}{d\tau} = -P_p g_c \frac{S_p}{c_p^*} \tag{13}$$

Assuming an ideal gas and an isothermal blowdown (a useful approximation but obviously incorrect in the strict sense), the breech pressure is given by the solution of Eq. (13)

$$(P_p/P_p^\circ) = \exp(-\alpha L\tau/a) \tag{14}$$

The corresponding mass flow from the pulser is

$$\dot{m}_p = \dot{m}_p^\circ \exp(-\alpha L\tau/a) \tag{15}$$

Note that the total mass of gas discharged by the pulser and, hence, the weight of the pulser powder charge can be obtained by integrating Eq. (15),

$$m_p = \dot{m}_p^\circ/\alpha \tag{16}$$

The Fourier transform of the pulser mass flow can be obtained from Eq. (15)

$$(\dot{m}_p/\dot{m}_p^\circ) = \left((\alpha L/a) + i\lambda\right)^{-1} \tag{17}$$

which can then be combined with Eq. (10) to obtain an equation for the Fourier transform of the aft end acoustic pressure.

Figure 3 shows the spectrum of the pulser flow for $(\alpha L/a) = 1$ and $\dot{m}_p^\circ/\dot{m}_c^\circ = 1.0$. The mass flow from this pulser decreases to 36.8% of its initial flow by the time the first pressure pulse reflects off the head end of the motor and returns to the aft end. This concentrates the oscillatory energy at frequencies below the fundamental acoustic frequency of the motor. Thus, one would expect this pulser to excite primarily the lower acoustic frequencies of the motor.

The spectra shown in Figs. 2 and 3 were combined and inverted using the inverse transforming capability of the spectrum analyzer to yield the pressure-time behavior shown in Fig. 4. Several interesting features of the waves are apparent. First, the pressure oscillations at the ends are out of phase, as expected. The second is the steep fronted character of the waves. Recalling that the wave shape of the pulser flow rises very rapidly and then falls more slowly, it appears the predicted pressure wave shape preserves this character of the pulser. Thus, the predicted behavior is consistent with the experimental observations reported by Baum et al.[4]

These wave shapes raise an interesting point regarding the interpretation of possible nonlinear oscillations in motors. There is a tendency to associate steep fronted waves having high harmonic content, as well as shifts in the mean pressure, with nonlinear behavior. However, this analysis shows that steep fronted waves can be generated in a purely linear system. Therefore, steep fronted waves are not sufficient evidence to indicate nonlinear behavior.

A third observation from Fig. 4 is the relatively small amplitude (i.e., about 8%) generated by the pulse. Since the initial mass flow from the pulser equaled the steady-state mass flow from the motor, this represents the response to a relatively large mass flow pulse. However, the pulsed action is nearly complete before the pressure wave reflects of the head end and returns to the pulser. Thus, the low pulse amplitudes observed in the simulator for the small Inertial Upper Stage motor[2] and in the Booster Separation Motor,[1] though surprising at first, are probably reasonable.

Figure 4 shows some high-frequency jitter in the predicted curve. This may result from numerical noise or from the inversion routine. Thus, this jitter is not considered to be significant at this point.

Additional calculations were then made to examine the effect of the pulser decay time on the pressure response of the motor. Figure 5 shows the time domain response when the pulser time constant was reduced by a factor of 10 to 0.1. Note that the magnitude of the oscillating components is roughly unchanged from those in Fig. 4. From Eq. (16), this change also requires a factor of 10 increase in the powder charge to maintain the same mass flow ratio. However, the bulk mode (i.e., low-frequency) response increased significantly. This change also has a very important practical implication. The

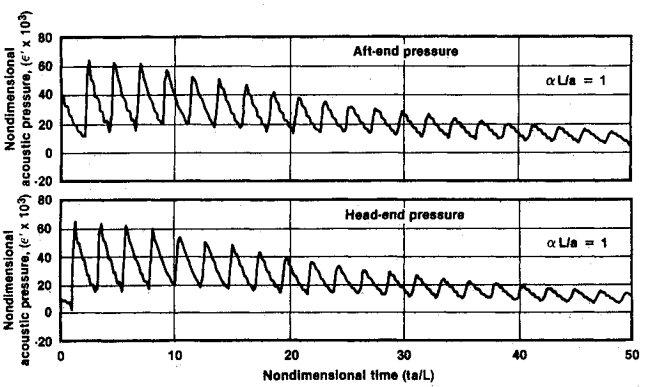

Fig. 4 Predicted acoustic pressure.

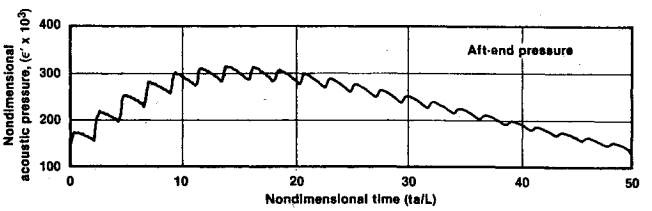

Fig. 5 Predicted acoustic pressure.

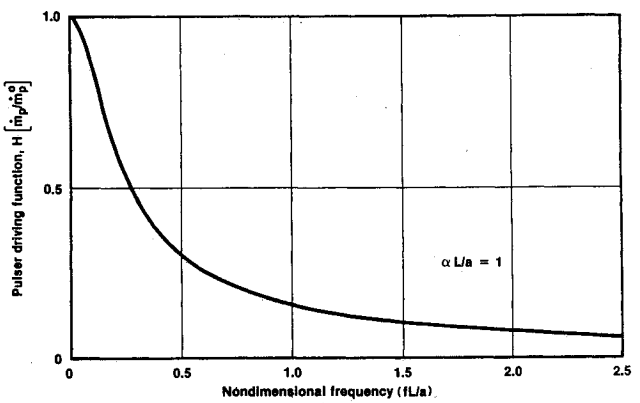

Fig. 3 Linear spectrum of pulser flow.

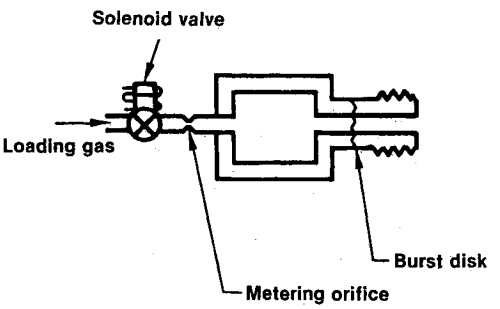

Fig. 6 Cold-flow pulser.

piezoelectric transducers used to measure these pressures in motors also respond to these low-frequency components, as well as the acoustic frequencies. Thus, the large excursion could saturate the recording system if it were ranged for the response at the acoustic frequencies alone. To prevent the saturation requries a decrease in the sensitivity of the recording system that compromises the signal-to-noise ratio. Therefore, long (compared to the period of the wave) pulsed decay times should be avoided.

Design Considerations

This analysis can also be used to develop design guidelines for blowdown (powder) pulsers. For design purposes, Eqs. (6) and (17) can be combined to yield

$$\tilde{\epsilon}_1 = \frac{[\dot{m}_p^\circ/\alpha][L/\dot{m}_c^\circ a]}{(1+i2\pi f/\alpha)[T(\lambda,r)-0.5(\gamma-1)]} \tag{18}$$

The term $2\pi f/\alpha$ scales the pulser decay time to the frequency of interest in the motor. A reasonable value is to size the pulser so the $\alpha = 2f$. Lower values increase the bulk mode response and higher values degrade the energy input to the mode of interest. The factor $(\dot{m}_p^\circ L/\alpha \dot{m}_c^\circ a]$ can now be set to obtain the desired magnitude of the pulse (approximately). This cannot be done exactly because the pulse magnitude also depends on the dynamic response of the motor, which is unknown and is to be measured from the pulse decay time in the motor. At this point, $\dot{m}_p^\circ/\dot{m}_c^\circ = 1$ is recommended. The powder charge is then determined from Eq. (16). The pulser volume, exhaust area, and burst disk thickness can then be determined to give these desired parameters.

Table 2 Pulser and motor cold-flow test conditions ($\gamma = 1.4$, $\bar{M} = 0.0103$)

Test No.	Pulser decay rate $\alpha L/a$ Measured	Predicted	$\dot{m}_p^\circ/\dot{m}_c^\circ$
4	−1.05	−0.90	−1.44
5	−0.74	−0.55	−1.44
11	−1.05	−0.90	−2.05

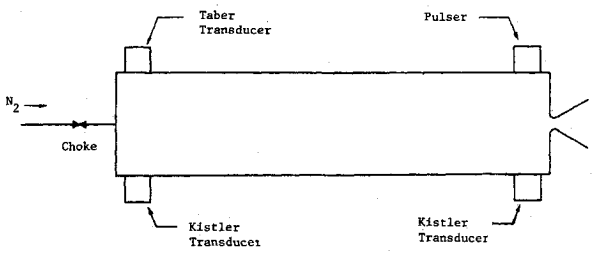

Fig. 7 Cold-flow test apparatus.

Cold-Flow Experiments

A series of cold-flow experiments was then conducted to test qualitatively these predictive methods under idealized conditions. The simple cold-flow blowdown pulser shown in Fig. 6 was fabricated and connected to the cold-flow apparatus shown schematically in Fig. 7. Tests were conducted at 230 psig using a 0.202 in. diameter throat in the exhaust nozzle and a chamber Mach number of 0.0103. Nitrogen entered the test chamber through a sonic choke. The pulse was generated by opening the solenoid valve to a high-pressure nitrogren supply, thereby slowly pressurizing the breech through a small sonic metering orifice. Once the shear strength of the burst disk was exceeded, the disk ruptured and the breech exhausted into the test chamber. Pressure transducers monitored the breech pressure as well as the static and oscillatory pressures in the test chamber.

There are several important differences in the acoustics between this apparatus and a real solid-propellant rocket motor. In this experiment, the mass addition is from the head end, rather than through the side walls. Thus, M is constant rather than increasing linearly with motor length. The boundary condition at the head end becomes one of constant mass flow, rather than zero acoustic velocity. With these changes, the solutions of Eqs. (1) and (2) for the aft end acoustic pressure becomes

$$\tilde{\epsilon}_1 = \frac{-\bar{M}(\dot{m}_p^\circ/\dot{m}_c^\circ)(\tilde{m}_p/\dot{m}_p^\circ)}{0.5\bar{M}(\gamma+1)+i\tan(\lambda)} \tag{19}$$

Three pulser tests were then conducted to provide a rough evaluation of the effect of the pulser parameters on the generated pressure oscillation. One test provided a baseline (test 4), one a reduced pulser decay rate (test 5), and one an in-

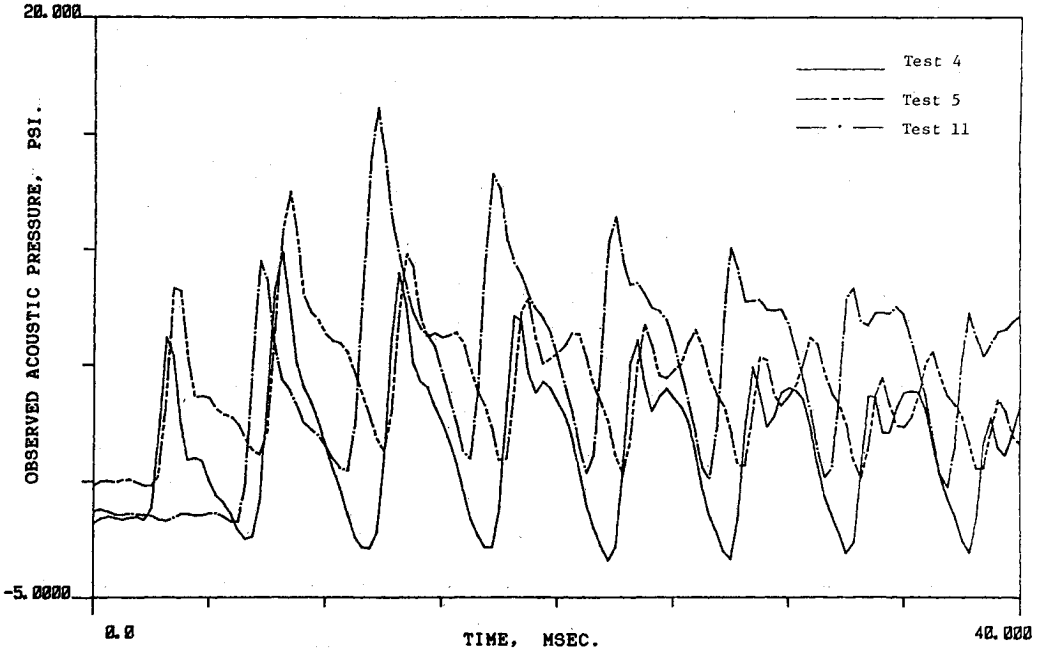

Fig. 8 Comparison of measured pulses.

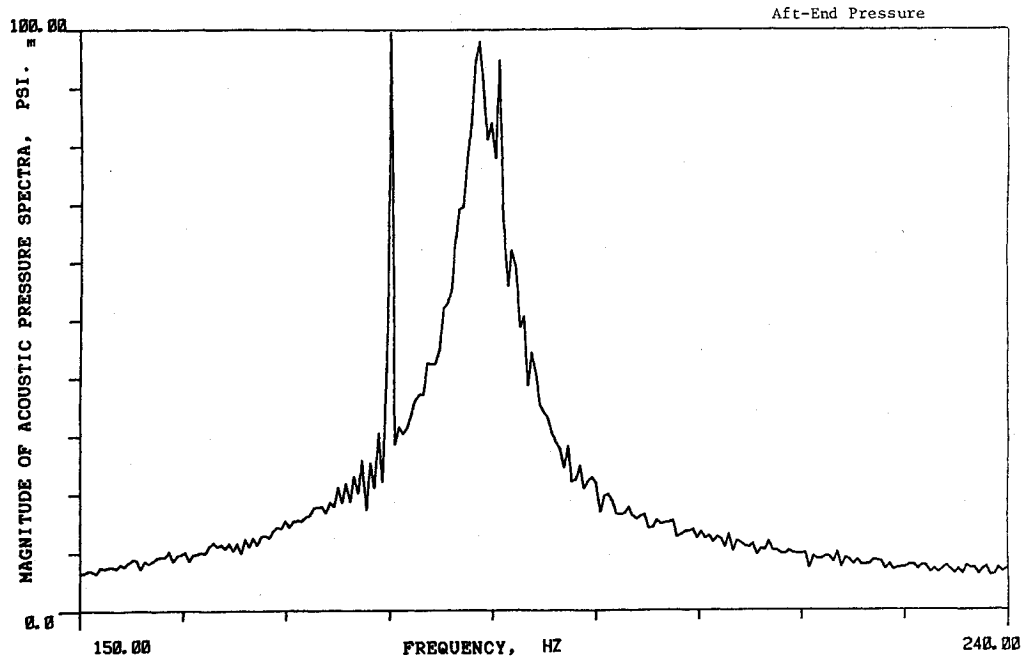

Fig. 9 Linear spectrum from cold-flow test.

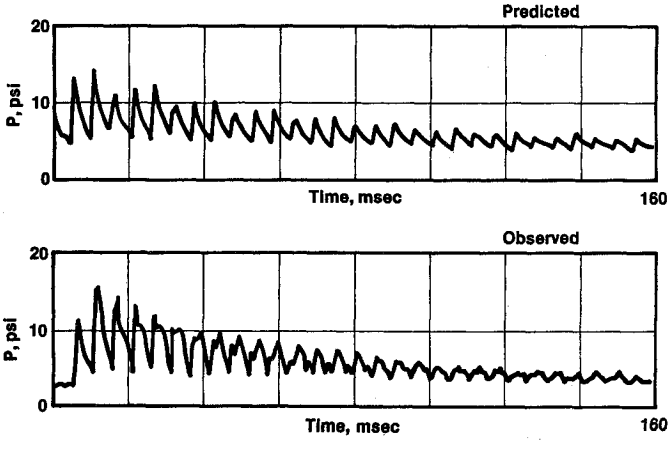

Fig. 10 Comparison of predicted and measured pulses.

creased initial mass flow rate from the pulser (test 11). These conditions are summarized in Table 2.

Figure 8 shows a comparison of the digitized aft end oscillatory pressures measured in these three tests. Comparing tests 4 and 5 shows that there is little effect on the pulse amplitude of decreasing the pulser decay time, as expected from the analysis. Comparing tests 4 and 11 shows that the initial amplitude increased by 47% with a 42% increase in the initial mass flow from the pulser. This observed amplitude increase agrees qualitatively with the predicted amplitude increase.

The measured pulse magnitudes were then compared with predicted values. In the first comparisons using Eq. (19) directly, the predicted amplitudes were approximately three times the observed amplitudes. As noted previously, the damping of the acoustic cavity is also an important factor in correctly predicting the acoustic pressure. Thus, damping in Eq. (19) was suspected as a possible source of the error.

The analytical acoustic model of this experiment [Eq. (19)] predicts the half-power bandwidth to be

$$Q=\pi/[\bar{M}(\gamma+1)]=127 \tag{20}$$

However, experimental measurements in this configuration[14,15] indicate that this prediction of Q may be high by as much as a factor of three. Therefore, the damping in the experimental apparatus was derived from the linear spectrum of the decaying pressure oscillations shown in Fig. 9. For an exponentially decaying signal, one can show that the magnitude of the corresponding Fourier transform is

$$\epsilon=[(\alpha L/a)^2+(\lambda-\lambda d)^2]^{-1/2} \tag{21}$$

This equation was curve fit to the measured spectrum from test 4 by the least squares method. The resulting Q was 38.9, which is roughly one-third the predicted value. It should be noted that the spectrum in Fig. 9 has a strong, but narrow, peak at 180 Hz. This peak was caused by a harmonic of the 60 Hz noise in the data and therefore was excluded from the curve fitting process.

Based on this comparison, Eq. (18) was modified to account for this increased damping by multiplying $\bar{M}$ by 127/38.9. Figure 10 shows a comparison of the predicted pulse with the observed pulse from test 11. Note that the prediction is reasonably close to, although slightly lower than, the experimental result. Several factors could account for this discrepancy. The numerical part of this analysis is limited to seven harmonics and, thus, it may suffer from accuracy limitations. The methods for correcting for the damping of the simulated motor may also introduce some errors. Considering the simplifications in the model, however, the agreement between the predictions and the measurements is considered quite good.

Conclusions

The results of this study have demonstrated the utility of a simplified analysis of blowdown pulsers. Simplified design guidelines have been derived that relate the blowdown time of the pulser to frequency of the oscillation to be tested. Specifically, the blowdown time should be twice the frequency of interest. In addition, the magnitude of the pulse scales directly with the ratio of initial pulser mass flow to the motor mass flow rate. Setting this ratio to unity is a reasonable starting point. However, uncertainties in the acoustic damping, which in fact is to be determined from the test results, make estimating the magnitude of the initial pulse difficult.

Acknowledgment

This work was sponsored by United Technologies through IR&D.

References

[1]Brown, R. S. and Deverall, L. I., "Combustion Stability Analysis for BSM," United Technologies Corp./Chemical Systems Div., East Hartford, CT, CSD Rept. RSB-14A-76R, 1976.

[2]Brown, R. S., Waugh, R. C., and Willoughby, P. G., "IUS Combustion Stability Studies," CPIA Pub. 329, Vol. III, pp. 297-325.

[3]Murray, J. A., Condon, J. A., and Krusch, D. E., "Pulsing Criteria for Solid Propellant Rocket Motors," AFRPL TR-79-45, March 1979.

[4]Baum, J. D., Lovine, R. L., and Levine, J. N., "Pulsing Techniques for Solid Propellant Rocket Motors: Modeling and Cold-Flow Testing," *Journal of Spacecraft and Rockets*, Vol. 20, March-April 1983, pp. 150-157.

[5]Baum, J. D., Levine, J. N., and Lovine, R. L., "Pulsed-Triggered Instability in Solid Rocket Motors," *AIAA Journal*, Vol. 22, Oct. 1984, pp. 1413-1419.

[6]Lovine, R. L., Baum, J. D., and Levine, J. N., "Ejecta Pulsing of Subscale Rocket Motors," AIAA Paper 83-0578, Jan. 1983.

[7]Culick, F. E. C., "Stability of Longitudinal Oscillations with Pressure and Velocity Coupling in a Solid Propellant Rocket," *Combustion Science and Technology*, Vol. 2, 1970, pp. 179-201.

[8]Culick, F. E. C., "The Stability of One-Dimensional Motions in a Rocket Motor," *Combustion Science and Technology*, Vol. 7, 1973, pp. 165-175.

[9]Brown, R. S. and Waugh, R. C., "Pressure and Velocity Response Function Measurements by the Rotating Valve Method," AGARD-CP-259, 1979, pp. 32-1—32-17.

[10]Abramowitz, M. and Stegum, I. A., "Handbook of Mathematical Functions with Tables, Graphs, and Mathematical Tables," NBS Science Publications, No. 55, June 1964, pp. 504-507.

[11]Brown, R. S., Waugh, R. C., and Kelly, V. L., "Rotating Valve for Velocity Coupled Combustion Response Measurements," *Journal of Spacecraft and Rockets*, Vol. 19, Sept.-Oct. 1982, pp. 437-444.

[12]Culick, F. E. C., "A Review of Calculations for Unsteady Burning of a Solid Propellant," *AIAA Journal*, Vol. 6, Oct. 1968, pp. 2241-2255.

[13]Brown, R. S. and Waugh, R. C., "Rotating Valve for Velocity Coupled Combustion Response Measurements," AFSOR-TR-80-0055, 1979.

[14]Buffum, F. G. Jr., Dehority, G. I., Slates, R. O., and Price, E. W., "Acoustic Attenuation Experiments on Subscale Cold-Flow Rocket Motors," *AIAA Journal*, Vol. 5, 1967, pp. 272-280.

[15]Jensen, G. E., "Nozzle Acoustic Loss Measurements," United Technologies Corp./Chemical Systems Div., Rept. CSD TM-36-73-U2, 1973.